Charge transport in organic semiconductors: Assessment of the mean field theory in the hopping regime

ARTICLE *in* THE JOURNAL OF CHEMICAL PHYSICS · AUGUST 2013

Impact Factor: 2.95 · DOI: 10.1063/1.4817856 · Source: PubMed

2 AUTHORS:

Linjun Wang
University of Southern California
49 PUBLICATIONS **1,152** CITATIONS
SEE PROFILE

David Beljonne
Université de Mons
355 PUBLICATIONS **15,080** CITATIONS
SEE PROFILE

Charge transport in organic semiconductors: Assessment of the mean field theory in the hopping regime

Linjun Wang[a] and David Beljonne
Laboratory for Chemistry of Novel Materials, University of Mons, Place du Parc 20, B-7000 Mons, Belgium

(Received 16 May 2013; accepted 25 July 2013; published online 14 August 2013)

The performance of the mean field theory to account for charge transfer rate in molecular dimers and charge transport mobility in molecular stacks with small intermolecular electronic coupling and large local electron-phonon coupling (i.e., in the hopping regime) is carefully investigated against various other approaches. Using Marcus formula as a reference, it is found that mean field theory with system-bath interaction and surface hopping approaches yield fully consistent charge transfer rates in dimers. However, in contrast to the dimer case, incorporating system-bath interaction in the mean field approach results in a completely wrong temperature dependence of charge carrier mobility in larger aggregates. Although the mean field simulation starting from the relaxed geometry of a charged molecule and neglecting system-bath interaction can reproduce thermally activated transport, it is not able to characterize properly the role of additional nonlocal electron-phonon couplings. Our study reveals that the mean field theory must be used with caution when studying charge transport in the hopping regime of organic semiconductors, where the surface hopping approach is generally superior. © *2013 AIP Publishing LLC*. [http://dx.doi.org/10.1063/1.4817856]

I. INTRODUCTION

Due to the rapid developments in the field of organic (opto)electronics, the theory of charge transport in organic semiconductors has been the subject of extensive investigations in the past decades.[1–28] It is well known that the coupling between electrons and phonons is critical to understand the intrinsic temperature dependence of mobility, which is widely used as a fingerprint for the charge transport mechanisms. Electron-phonon couplings have two flavors, namely, the local couplings that characterize the dependence of local electron energy on nuclear positions and the nonlocal electron-phonon couplings that account for the dependence of intermolecular electron coupling on the relative distance between adjacent molecules. In the most general cases, both the low and high frequency vibrational modes have contributions to both local and nonlocal electron-phonon couplings.[7] However, recent studies have confirmed that only low frequency modes are important for the temperature dependence of mobility in organic materials, while the high frequency vibrations only contribute a temperature-independent renormalization factor to the intermolecular electron coupling due to their low occupation number at usual temperatures.[6,7] A reasonable approximation consists in carrying out single molecular analysis to obtain the electron-phonon couplings related to the high frequency intra-molecular modes, while the low frequency fluctuations of the electron site energies and electron couplings between adjacent molecules are sampled from molecular dynamics simulations on molecular crystals or aggregates.[14,17] The charge transport properties can then be calculated through a mixed quantum-classical dynamics (MQCD),[18–23] which treats the nuclear motions classically and the electron dynamics quantum mechanically. This approach enables to study complex electron-phonon interactions numerically with good accuracy and at reasonable computational cost.

The MQCD is often carried out using either the mean-field (MF) (or Ehrenfest) approach[29–32] or by means of surface-hopping (SH) algorithms.[33,34] In both cases, the electron wave function responds rigorously to the nuclear motion through solving the time-dependent Schrödinger or the Liouville equations as a function of the dynamic nuclear configuration. The difference between MF and SH methods lies mainly in the description of the classical nuclear equation of motion. The nuclear evolution in the MF theory is governed by the gradient of the expectation value of the energy from the time dependent electron wave function, namely, a single average potential energy surface. In contrast, the SH approach can incorporate nonadiabatic transitions between different adiabatic potential energy surfaces, considering the fact that nuclear evolution on sufficiently different adiabatic energy surfaces may lead to divergent trajectories. Due to its simplicity, the MF theory is still widely used for charge transport in organic materials.[18–23] Although the advantages and limitations of MF theory have been well documented for general applications,[30] a systematic understanding of its performance in charge transport is still lacking. We note that the applicability of the MF and SH methods depends strongly on the decoherence time of the investigated system, namely, MF is exact in the limit of infinite decoherence time while SH implies a finite decoherence time; we here focus on the performance of MF and SH within the scope of the hopping regime of charge transport.

Starting from Holstein's seminal work in 1959,[1] the polaron model for charge transport in molecular crystals has been extensively studied.[2–11] If the intermolecular electronic coupling is much stronger than the electron-phonon

[a]Email: linjun.wang@umons.ac.be

coupling strength, the Holstein model goes to the band transport limit.[16] In this case, charge transport is dominated by delocalized states with a narrow distribution of the electron momentum, and thus the MF theory should be optimal as pointed out previously.[23] In the other limit of weak intermolecular electronic coupling and strong electron-phonon coupling, the electron tends to hop between localized states behaving as a small polaron and the thermally activated temperature dependence of mobility can be derived analytically from perturbation theories.[6,9] The hopping process entails the electron having enough time for thermal relaxation after each hop, and thus a very relevant quantity is the charge transfer rate in molecular dimers. The full quantum expressions based on the Fermi Golden Rule (FGR)[35] and the classical approximated Marcus formula[36] have been widely used together with the Pauli master equation (PME) or the kinetic Monte-Carlo (KMC) algorithm to calculate hopping mobility.[26] Recently, it was found that SH with proper treatment of the decoherence can recover the correct scaling predicted by the Marcus formula.[34] Using these existing analytical results as reference, we can examine the performance of the MF theory not only for charge transfer rate between molecular dimers but also for charge transport mobility in organic solids. We will especially focus on the temperature dependence as a marker for the charge transport mechanism.

In this paper, we will also cover some other closely related aspects. (1) We notice that, in a lot of MF studies on charge transport, the initial nuclear coordinates simply follow a Boltzmann distribution based on the neutral molecular geometry.[18–23] This is reasonable for systems with large mobility, but is questionable in the limit of small electronic coupling and strong local electron-phonon coupling, where the presence of a charge is accompanied by a distortion of the molecular structure. We will investigate the impact of different initial nuclear configurations on the transport properties. (2) For charge transport in real materials, the system-bath interaction, which allows heat transfer between the charged molecules and the environment, could be quite important for the self-localization and transport dynamics of the charge. In this study, the system-bath interaction will be included using the Langevin model, namely, by adding a friction term and random forces to the nuclear equations of motion. (3) Due to the softness of organic materials and the fact that electronic couplings are strongly related to the intermolecular orientation, the nonlocal electron-phonon coupling in organic semiconductors is generally very large.[7,17] Recently, MQCD simulations have been used to study the charge transport in pentacene crystals with pure nonlocal electron-phonon couplings in the absence of local electron-phonon couplings.[18] It was found that the thermal fluctuation to the electronic couplings lifts the crystal symmetry, resulting in dynamical charge localization but with a bandlike temperature dependence of mobility. Hereby, we will investigate the role of nonlocal electron-phonon coupling on charge transport with the presence of strong local electron-phonon couplings. (4) A recently developed flexible surface hopping (FSH) approach,[37] which can reproduce the transition from hopping to bandlike transport in organic crystals with the increase of the intermolecular electronic couplings, is also applied and the results are compared with the mean field methods to check the importance of nonadiabatic transitions in charge transport.

II. THEORETICAL METHODOLOGY

In Secs. II A and II B, we first describe the approaches to obtain the charge transfer rate between adjacent molecules, including analytical methods (FGR and Marcus formulas) and MQCD numerical approaches (SH and MF theories). Then we move to the charge transport theories for molecular stacks, namely, the PME and the KMC approaches based on charge transfer rates, the small polaron model, the FSH approach, and the MF theory. Note that all the analytical methods used in this study work in the limit of small intermolecular electronic couplings with respect to reorganization energies, and Marcus theory additionally applies to the high temperature limit. Although this study only focuses on one-dimensional stacks, these methods can be easily extended to higher dimensions.

A. Molecular dimer model

In organic semiconductors comprising a single type of conjugated molecules, charge transfer processes between adjacent molecules are actually self-exchange reactions. The initial and final states for electron transfer can be represented as R^-R and RR^-, respectively, with R^- denoting the electron on molecule R. We consider only one reaction coordinate, x, and adopt the following spin-boson Hamiltonian in the basis of diabatic states,

$$H = \begin{pmatrix} \frac{1}{2}m\omega^2x^2 + Mx & \tau \\ \tau & \frac{1}{2}m\omega^2x^2 - Mx \end{pmatrix}, \qquad (1)$$

where τ is the diabatic coupling between the two molecules, m and ω are the mass and the frequency of the nuclear vibration along the reaction path, respectively. The local electron-phonon coupling factor, M, can be expressed in terms of the reorganization energy, λ, as $M = \sqrt{\lambda m\omega^2/2}$.[34]

1. FGR and Marcus formulas for charge transfer rate

When the perturbation theory is applied in the small electronic coupling limit ($\tau \ll \lambda$), the quantum-mechanical expression for charge transfer rate can be derived from the FGR as[35]

$$k_{FGR} = \frac{\tau^2}{\hbar^2}\int_{-\infty}^{\infty} dt\ \exp\{-S[(2n+1) - ne^{-i\omega t} - (n+1)e^{i\omega t}]\}. \qquad (2)$$

Here, $n = 1/[\exp(\hbar\omega/k_BT) - 1]$ is the boson occupation number of the phonon mode, k_B is the Boltzmann constant, T is the temperature, and $S = \lambda/\hbar\omega$ is the Huang-Rhys factor measuring the coupling strength between the charge carrier and the vibrational mode. In the strong coupling ($S \gg 1$) and high temperature ($k_BT \gg \hbar\omega$) limits, the short-time approximation can be applied, and then Eq. (2) goes to the widely used semiclassical Marcus charge transfer rate,[36]

$$k_{Marcus} = \frac{\tau^2}{\hbar}\sqrt{\frac{\pi}{\lambda k_BT}}\exp\left(-\frac{\lambda}{4k_BT}\right). \qquad (3)$$

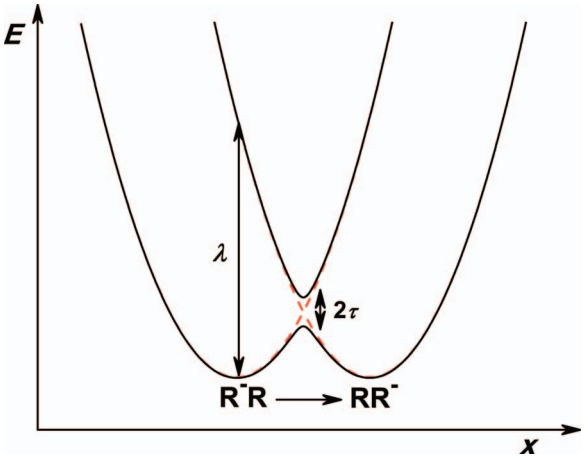

FIG. 1. Schematic representation of the potential energy surfaces related to an electron transfer process in a molecular dimer, together with the corresponding reorganization energy, λ, and the diabatic electronic coupling, τ. The two diabatic states are shown with red dashed lines, while the two adiabatic states are shown with black solid lines.

2. SH approaches for charge transfer rate

Following Tully's standard "fewest switches" algorithm,[33] we perform the SH dynamics in the adiabatic basis. Diagonalizing the Hamiltonian in Eq. (1), we can get the adiabatic energy surfaces (see Fig. 1),[34]

$$E_{1,2}(x) = \frac{1}{2}m\omega^2 x^2 \mp \sqrt{M^2x^2 + \tau^2}, \tag{4}$$

where surface 1 (2) represents the lower (higher) adiabatic surface which takes the minus (plus) sign and the adiabatic states in terms of the left and right diabatic states, $|\phi_l\rangle$ and $|\phi_r\rangle$,

$$|\Phi_{1,2}(x)\rangle = \sqrt{\frac{1}{2} \mp \frac{1}{2}\frac{Mx}{\sqrt{M^2x^2+\tau^2}}}|\phi_l\rangle \mp \sqrt{\frac{1}{2} \pm \frac{1}{2}\frac{Mx}{\sqrt{M^2x^2+\tau^2}}}|\phi_r\rangle, \tag{5}$$

We define the wave function as a linear expansion of the adiabatic states, $\Phi(x) = c_1\Phi_1(x) + c_2\Phi_2(x)$. According to the Schördinger equation, we have[33]

$$\dot{c}_i = \frac{1}{i\hbar}c_i E_i - \sum_{j\neq i} c_j \dot{x} \cdot d_{ij}. \tag{6}$$

Here $d_{ij}(x) \equiv \langle \Phi_i(x)|\mathrm{d}\Phi_j(x)/dx\rangle$ are nonadiabatic couplings. We obtain[34]

$$d_{12}(x) = \frac{1}{2}\frac{M\tau}{M^2x^2+\tau^2}, \tag{7}$$

and note that $d_{21} = -d_{12}$, and $d_{11} = d_{22} = 0$.[33] In realistic organic systems, there are a lot of nuclear vibrational modes. However, we include only one effective mode in the model, and thereby all the other modes can be regarded as an effective bath reacting on this mode. The nuclear equation of motion is thus modeled by a Langevin equation to take system-bath interaction into account,

$$m\ddot{x} = -dE_a/dx - \gamma m\dot{x} + \xi. \tag{8}$$

Here a represents the active surface, γ is the friction coefficient, ξ is a Markovian Gaussian random force with standard deviation $\sqrt{2\gamma m k_B T/\Delta t}$, and Δt is the time step of the dynamics.[34] We solve Eq. (6) numerically through the standard fourth-order Runge-Kutta (RK4) algorithm,[38] and Eq. (8) also at the RK4 level following the work by Hershkovitz (see the Appendix).[39]

In each realization, we initially choose a Boltzmann distribution of nuclear position and velocity in the left diabatic state. The corresponding electronic amplitudes, c_i, and the initial probability on each adiabatic surface are calculated based on Eq. (5).[34] The evolution of the electron wave function and nuclear coordinates is carried out according to Eqs. (6) and (8), respectively. The switching probabilities from adiabatic surface i to adiabatic surface j is $g_{ij} = \Delta t \cdot 2\mathrm{Re}(c_i c_j^* v d_{ij})/c_i^* c_i$, which is reset equal to zero if $g_{ij} < 0$. We generate a uniform random number, ζ, and make a switch from i to j if $\zeta < g_{ij}$. Besides, if $E_i + mv^2/2 > E_j$, a velocity adjustment is made in order to conserve the total energy, $v' = v\sqrt{1 + (E_i - E_j)/(mv^2/2)}$; otherwise the switch is not activated.[33] If a switch has occurred, the trajectory will then evolve on the potential energy surface E_j. The population on the left diabatic surface is recorded, and the time evolution of the average population after a certain number of separate realizations for electron and nuclear dynamics is used to get the charge transfer rate through a fit to an exponential function, $f = a\exp(-kt) + b$, where k is the charge transfer rate to be fitted.[34] In general, the decoherence time can be evaluated from the auto-correlation function of the site energies.[40] Using a short time approximation, a simple formula can be derived based on the Eq. (1) for the decoherence time, i.e., $t_{decoherence} = \frac{\hbar}{M}\sqrt{\frac{m\omega^2}{2k_BT}}$, where k_B is the Boltzmann constant and T is the temperature. However, SH with decoherence (SHD) in this study is performed simply by collapsing the electronic wave function whenever the trajectory crossed the minimum of a diabatic well while moving away from the crossing point.[34] More explicitly, each time the position of a trajectory crossed $x = \pm M/m\omega^2$ on the lower adiabatic surface, we set $c_1 = 1$ and $c_2 = 0$, forcing all the probability density on the lower surface.

3. MF approach for charge transfer rate

In the MF approach, we carry out the dynamics simulations in diabatic basis and express the electron wave function as $\Phi = c_l|\phi_l\rangle + c_r|\phi_r\rangle$. The first derivative of the wave function is calculated by the Schrödinger equation $\dot{\Phi} = H\Phi/i\hbar$, and the acceleration of the classical degree of freedom is obtained through the spatial derivative of the potential energy $\dot{v} = -\frac{1}{m}\partial\langle\Phi|H|\Phi\rangle/\partial x$. More explicitly,

$$\dot{c}_l = (Mxc_l + \tau c_r)/i\hbar, \tag{9}$$

$$\dot{c}_r = (\tau c_l - Mxc_r)/i\hbar, \tag{10}$$

$$\dot{v} = -\omega^2 x + M(c_r^* c_r - c_l^* c_l)/m. \tag{11}$$

The charge transfer rate is obtained through the same exponential fit procedure of the time-dependent population on

the left diabatic surface, $c_l^* c_l$. When system-bath interaction is included, the MF with Langevin equation (MFL) can be carried out similarly as for the SH method.

B. Molecular stack model

We consider a one-dimensional model system containing N molecular sites with periodic boundary conditions. In order to take into account both local and nonlocal electron-phone couplings, we set each molecule k with two intramolecular vibrational degrees of freedom $x_{k,1}$ and $x_{k,2}$ with force constants K_1 and K_2 as well as effective masses m_1 and m_2. The corresponding velocities are $v_{k,1}$ and $v_{k,2}$. The electronic state that has a localized carrier on the molecule k is denoted as $|k\rangle$, e.g., the highest occupied molecular orbital for hole transport, and the lowest unoccupied molecular orbital for electron transport. At equilibrium geometry, the electronic coupling between the localized states of the nearest neighbors is $-\tau$, and the onsite energies of all the molecular states are the same, therefore set to zero for simplicity. The onsite energy of molecule k is linearly modulated by $x_{k,1}$ with the local electron-phonon coupling constant α, and the electronic coupling between molecule k and its neighboring molecule $k+1$ is linearly modulated by $x_{k+1,2} - x_{k,2}$ with the nonlocal electron-phonon coupling constant β. The mixed quantum-classical Hamiltonian can be expressed as

$$\begin{aligned} H = & \sum_k \alpha x_{k,1} |k\rangle\langle k| + \sum_k \left(m_1 v_{k,1}^2 + K_1 x_{k,1}^2\right)/2 \\ & + \sum_k [-\tau + \beta(x_{k+1,2} - x_{k,2})](|k\rangle\langle k+1| + |k+1\rangle\langle k|) \\ & + \sum_k \left(m_2 v_{k,2}^2 + K_2 x_{k,2}^2\right)/2. \end{aligned} \tag{12}$$

1. PME and KMC for charge transport mobility

The PME[41] is a frequently used model to study charge transport processes in organic semiconductors. It can be derived from elementary quantum mechanics along with a Markov assumption. It constitutes a set of purely classical kinetic equations describing the evolution of the electron population at each state,

$$\dot{P}_i = \sum_j (k_{ji} P_j - k_{ij} P_i), \tag{13}$$

VIP: writing mistake: correct equation is lambda=alpha^2/K_1

where P_i is the occupation number of the charge to be on molecule i, and k_{ij} is the charge transfer rate from molecule i to j (the reorganization energy is $\lambda = \sqrt{\alpha^2/K_1}$). The PME can be solved through an iterative numerical scheme or a KMC algorithm. In the former approach, the population at time zero on one molecule is set to be unity, while the others are zero. The time evolution of the populations can be obtained through RK4.[38] The mean-square displacement (MSD) reads

$$MSD(t) = \sum_i P_i(t)(iL)^2 - \left[\sum_i P_i(t) iL\right]^2, \tag{14}$$

where L is the intermolecular distance. In normal diffusive regime, there is a linear relationship between MSD and the simulation time. Then the diffusion coefficient can be evaluated through the time derivative of the MSD as

$$D = \frac{1}{2n} \lim_{t\to\infty} \frac{dMSD}{dt}, \tag{15}$$

where n is the space dimension. Finally, the carrier mobility can be calculated by means of the Einstein relation:[42,43]

$$\mu = \frac{e}{k_B T} D. \tag{16}$$

The KMC approach to simulate the charge transport mobility is actually a random walk simulation.[26] An arbitrary site is initially chosen as the starting position for the charge. For a stack containing only one molecular species, the charge transfer rate to the left neighbor is the same as that to the right neighbor, which is denoted as k, and thus the charge has a probability of 1/2 to hop left or right. In practice, in order to identify the next site for the charge in a statistical sense, a random number ζ uniformly distributed between 0 and 1 is generated. If $\zeta < 1/2$, the charge hops to the right neighbor after a waiting time of $1/2k$; otherwise it hops to the left neighbor. The simulation continues until the diffusion distance is sufficient long, and this simulation is repeated a few thousand times. When we get a linear time dependence of the MSD, the mobility can be calculated according to Eqs. (15) and (16).

2. Small polaron model for charge transport mobility

The small polaron model starts from the fully quantum version of the mixed quantum-classical Hamiltonian in Eq. (12),

$$\begin{aligned} H = & \sum_k g_1 \hbar\omega_1 \left(b_{k,1}^+ + b_{k,1}\right)|k\rangle\langle k| + \sum_k \hbar\omega_1 (b_{k,1}^+ b_{k,1} + 1/2) \\ & + \sum_k [-\tau + g_2 \hbar\omega_2 (b_{k,2}^+ + b_{k,2})](|k\rangle\langle k+1| + |k+1\rangle\langle k|) \\ & + \sum_k \hbar\omega_2 (b_{k,2}^+ b_{k,2} + 1/2). \end{aligned} \tag{17}$$

Here, $b_{k,1}^{(+)}$ and $b_{k,2}^{(+)}$ represent annihilating (creating) a phonon related to modes $x_{k,1}$ and $x_{k,2}$, respectively. The corresponding phonon frequencies are $\omega_1 = \sqrt{K_1/m_1}$ and $\omega_2 = \sqrt{K_2/m_2}$. The dimensionless local and nonlocal electron-phonon coupling constants are $g_1 = \alpha/\omega_1\sqrt{2m_1\hbar\omega_1}$ and $g_2 = \beta/\omega_2\sqrt{m_2\hbar\omega_2}$. The small polaron mobility can be expressed as[6]

$$\mu = \frac{eL^2}{k_B T \hbar^2} \int_{-\infty}^{+\infty} dt\, \chi(t) e^{-2g_1^2[(1+2n_1)(1-\cos\omega_1 t) + i\sin\omega_1 t] - 2g_2^2[(1+2n_2)(1-\cos\omega_2 t) + i\sin\omega_2 t]}. \tag{18}$$

Here $\chi(t)=\tau^2+g_2^2\hbar^2\omega_2^2[(1+n_2)\exp(-i\omega_2 t)+n_2\exp(i\omega_2 t)]/2$, n_1 and n_2 are the occupation numbers of the two phonon modes.

3. FSH approach for charge transport mobility

Similar to the SH procedure for a molecular dimer, we diagonalize the electron Hamiltonian in Eq. (12) to get the adiabatic states in terms of the original diabatic orbitals $\{\Phi_i=\sum_k p_{ki}|k\rangle\}$ and the corresponding energies $\{E_i\}$. The electron wave function is expressed as a linear expansion of these adiabatic states, $\Phi=\sum_i c_i\Phi_i$. The equations of motion for the charge and the nuclei are written as[37]

$$\dot{c}_i=\frac{1}{i\hbar}c_iE_i-\sum_{j\neq i}c_j\sum_k\left(\dot{x}_{k,1}\cdot d_{ij}^{k,1}+\dot{x}_{k,2}\cdot d_{ij}^{k,2}\right), \quad (19)$$

$$m_{1(2)}\ddot{x}_{k,1(2)}=-V'_{k,1(2)}-\gamma m_{1(2)}\dot{x}_{k,1(2)}+\xi_{1(2)}, \quad (20)$$

where the nonadiabatic couplings $d_{ij}^{k,1(2)}$ and the spatial derivatives of the potential energy $V'_{k,1(2)}$ can be evaluated numerically by the Hellmann-Feynman theorem.[37,44] At this point, we notice that charge carriers involving weak intermolecular couplings as well as large electron-phonon couplings are generally delocalized over only a few molecules and only the surrounding nuclear vibrations are strongly coupled with the charge carrier. Therefore, it seems reasonable to describe this subsystem using costly SH dynamics while the rest of the system is simply treated in a classical manner.[37] Besides, such SH subsystem should be flexible along the dynamics with real time events of adding and/or removing neighboring molecules inside the subsystem. To check if a neighboring molecular orbital ($|j\rangle$) should be added to the SH subsystem, we regard the active state of the SH subsystem ($|\Phi_a\rangle=\sum_i p_{ia}|i\rangle$) and this test state together as a two-level system, and calculate their onsite energies and coupling by[37]

$$\langle\Phi_a|H_e|\Phi_a\rangle=\alpha\sum_i p_{ia}^2x_{i,1}+\sum_i 2[-\tau+\beta(x_{i+1,2}-x_{i,2})]p_{i+1,a}p_{ia}, \quad (21)$$

$$\langle j|H_e|j\rangle=\alpha x_{j,1}, \quad (22)$$

$$\langle\Phi_a|H_e|j\rangle=\alpha p_{ja}x_{j,1}+[-\tau+\beta(x_{j+1,2}-x_{j,2})]p_{j+1,a}+[-\tau+\beta(x_{j,2}-x_{j-1,2})]p_{j-1,a}. \quad (23)$$

When the absolute value of the ratio between the coupling and the energy difference is larger than a critical fraction R_c, we add the state $|j\rangle$ into the new SH subsystem, and a similar procedure is performed when removing a molecular orbital from the SH subsystem. When the SH subsystem is modified, the active state is changed to the adiabatic state of the new subsystem that mostly overlaps with the old active state. In addition, we also use a flexible time interval for the dynamics to increase the computational efficiency since the adiabatic states are strongly mixed in the nonadiabatic regimes. In detail, a proper time interval Δt is adjusted at each time step to ensure that the minimum overlap between the adiabatic state at time t and the corresponding adiabatic state at the next time step $t+\Delta t$ cannot be smaller than a certain critical value O_c. With this approach, smaller time steps are automatically generated when the dynamics is close to a nonadiabatic regime.

The initial nuclear coordinates and velocities are set from Gaussian distributions with variances of $k_BT/K_{1(2)}$ and $k_BT/m_{1(2)}$ for $x_{k,1(2)}$ and $v_{k,1(2)}$, respectively,[18,23] and the charge carrier placed on one molecule of the stack at time zero. The switching probability from the active adiabatic surface i to another adiabatic surface j is $g_{ij}=\Delta t\cdot 2\mathrm{Re}[c_ic_j^*\sum_k(v_{k,1}d_{ij}^{k,1}+v_{k,2}d_{ij}^{k,2})]/c_i^*c_i$,[37] which is reset equal to zero in case $g_{ij}<0$. For each surface j, we generate a uniform random number ζ, and make a surface hop from i to j if $\zeta<g_{ij}$. If $E_i+\sum_k(m_1v_{k,1}^2+m_1v_{k,1}^2)/2>E_j$, the hop is successful, and a velocity adjustment is made in order to conserve the total energy of the system,[37] $v'_{k,1(2)}=v_{k,1(2)}+d_{ij}^{k,1(2)}A/B\cdot[-1+\sqrt{1+2(E_i-E_j)B/A^2}]$, where $A=\sum_k(m_1v_{k,1}d_{ij}^{k,1}+m_2v_{k,2}d_{ij}^{k,2})$ and $B=\sum_k(m_1d_{ij}^{k,1}\cdot d_{ij}^{k,1}+m_2d_{ij}^{k,2}\cdot d_{ij}^{k,2})$. Suppose the hopping process took place, the trajectory now evolves on the potential energy surface E_j. Based on a recent work by Bittner *et al.*,[45] decoherence is achieved by collapsing the electronic wave function after every successful and unsuccessful hop. It means that the average frequency of hops sets the decoherence time, which can be estimated by the inverse of the charge transfer rate in molecular dimers. This is a reasonable approximation close to the incoherent hopping regime. For each realization m, the time evolution of the active state $\Phi_a^{(m)}(t)$ is restored, and used to calculate the MSD after a total number of M' realizations,

$$MSD(t)=\frac{1}{M'}\sum_{m=1}^{M'}\left[\left\langle\Phi_a^{(m)}(t)\middle|r^2\middle|\Phi_a^{(m)}(t)\right\rangle-\left\langle\Phi_a^{(m)}(t)\middle|r\middle|\Phi_a^{(m)}(t)\right\rangle^2\right]. \quad (24)$$

The matrix elements can be computed from the relations $\langle k|r^2|l\rangle=\delta_{kl}k^2L^2$ and $\langle k|r|l\rangle=\delta_{kl}kL$. When the MSD shows a linear evolution in time, one enters equilibrium diffusion and the mobility can be evaluated.

4. MF approach for charge transport mobility

The system Hamiltonian $H(t)$ at any given time t can be determined from Eq. (12) based on the coordinates and velocities of the classical degrees of freedoms. If the wave function $\psi(t)=\sum_k\psi_k|k\rangle$ is used to express a pure electronic state of the system, we can get the acceleration of any classical degree of freedom through the spatial derivative of the system energy $\dot{v}_k(t)=-\frac{1}{m}\partial\langle\psi(t)|H(t)|\psi(t)\rangle/\partial x_k$ and the first derivative of the wave function by the Schrödinger equation $\dot{\psi}(t)=H(t)\psi(t)/i\hbar$. We then obtain:

$$\dot{\psi}_k=\{\alpha x_{k,1}\psi_k-\tau(\psi_{k+1}+\psi_{k-1})+\beta[(x_{k,2}-x_{k-1,2})\psi_{k-1}+(x_{k+1,2}-x_{k,2})\psi_{k+1}]\}/i\hbar, \quad (25)$$

$$\dot{v}_{k,1}=(-K_1x_{k,1}-\alpha\psi_k^*\psi_k)/m_1, \quad (26)$$

$$\dot{v}_{k,2}=[-K_2x_{k,2}+\beta(\psi_k^*\psi_{k+1}+\psi_{k+1}^*\psi_k-\psi_{k-1}^*\psi_k-\psi_k^*\psi_{k-1})]/m_2. \quad (27)$$

With these differential equations, all the corresponding dynamical properties can be solved iteratively with the RK4 method.[38]

As for the SH approach, the coordinates and velocities, $\{x_{k,1(2)}\}$ and $\{v_{k,1(2)}\}$, are initially sampled from Boltzmann distributions. We put the carrier locally on one molecule at time zero, which is labeled as molecule 1. If we use the neutral structure as the initial geometry of this molecule, the mean value for $x_{1,1}$ is zero; when the charged structure is used as initial configuration instead, $x_{1,1}$ is set to $-\alpha/K_1$. We obtain the time dependent wave function $\psi_m(t)$ for each realization m, calculate the MSD similar to Eq. (24) and the carrier mobility by means of Eqs. (15) and (16). System-bath interaction can be added with similar approaches as for charge transfer rate described above.

III. RESULTS AND DISCUSSION

A. Parameters

Based on earlier work for charge transport in molecular crystals,[18,23] we adopted the following set of parameters: $\tau = 50$ cm^{-1}, $\alpha = 3500$ cm^{-1}/ Å, $K = 14500$ amu/ps^2, and $m = 250$ amu, for both charge transfer rate and charge transport mobility calculations accounting only for local electron-phonon couplings. Here, the frequency of the mode and the reorganization energy are calculated to be about 40 cm^{-1} and 1011 cm^{-1}, respectively; these are typical values for molecular crystals.[23] For convenience, the same K and m are used when we study the role of nonlocal electron-phonon couplings. The time interval in all simulations is chosen to be 0.1 fs, which has been carefully checked to yield a good balance between accuracy and computational cost. For charge transport, the system size for charge transport is at least 300 sites in MF calculations depending on the temperature of the system, while a system size of 50 in SH studies is enough to get equilibrium diffusion in the absence of boundary effects. Depending on the time-dependent behavior of electron dynamics, the total simulation time is 10 ps for charge transfer rate studies, and 500 ps and 2 ps for charge transport studies using MF and SH methods, respectively. The intermolecular distance is set to be $L = 5$ Å, consistent with typical values in organic molecular crystals. We set $R_c = 1/15$ and $O_c = 0.9999$ to ensure flexible but reliable SH dynamics for charge transport.[37] More than 10 000 realizations are performed to get a smooth time dependent population and time evolution of the MSD for equilibrium diffusion. The highest temperatures investigated for charge transfer rate and charge transport mobility are 5000 K and 1000 K, respectively. These high temperatures, which might not be realistic in actual organic solids, are meant to theoretically investigate the mobility dependence near crossover temperatures.

B. Charge transfer rate in molecular dimers

We first investigate the role of γ on the charge transfer rate between two molecules. In the literature, Kramer's theory predicts that the rate increases in the under-damped limit for small γ, levels off at the transition state regime for moderate γ, and then decreases in the over-damped limit when γ gets very large.[46] Our calculated SH charge transfer rate in the absence of decoherence at different temperatures as a function of γ are fully consistent with Kramer's theory, see Fig. 2(a). For temperatures less than 500 K, a transition state regime is at play. A value of $\gamma = 4$ ps^{-1} is used below as the reference parameter in SH and MF calculations of charge transfer rates. We should mention that the temperature dependence of charge transfer rate, which is the main focus of the present study, seems to be quite insensitive to the choice of γ (see Fig. 2(b)).

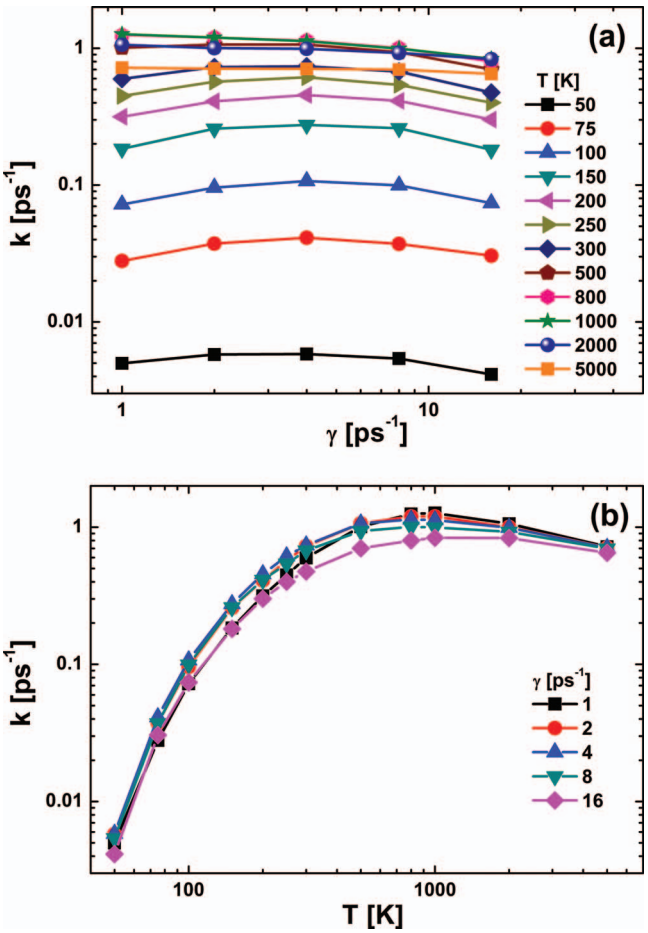

FIG. 2. (a) Friction and (b) temperature dependence of the charge transfer rate by the SH approach without decoherence.

In Fig. 3(a), we show the time evolution of the charge population on the left molecular site calculated by MF, MFL, SH, and SHD approaches. We find that SHD and SH give almost identical results, showing that the decoherence effect is not relevant here. This result seems to be in contradiction with a recent publication,[34] where Landry and Subotnik pointed out that a proper treatment of decoherence should be taken into account in the SH approach to yield the correct scaling with the electronic coupling. We argue that this study mainly investigated the charge transfer rate around the "inverted Marcus regime," where the Gibbs free energy difference between the right and the left molecular site is close to the reorganization energy. This strongly differs from the case studied here, as the Gibbs free energy is zero for self-exchange.

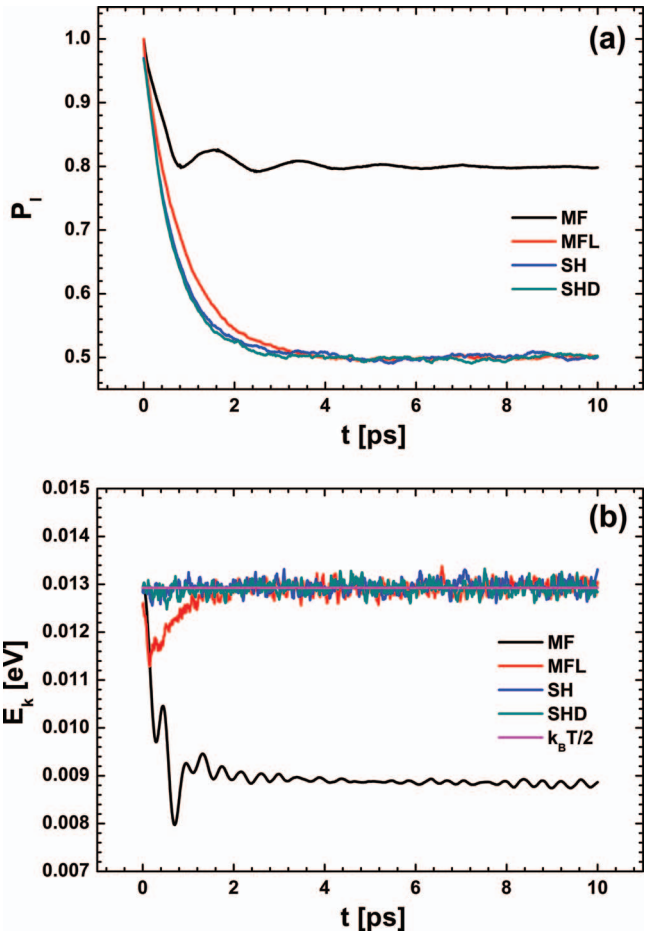

FIG. 3. Time evolution of (a) the charge population on the left molecule in the dimer and (b) total kinetic energy of the dimer, using the MF theories with and without system-bath interaction, as well as SH approach with and without decoherence.

Besides, it was found that the role of the decoherence gets smaller with increasing the electronic coupling, and becomes negligible when the electron coupling is larger than 1% of the reorganization energy.[34] This is the case in this study: the electronic coupling is 50 cm^{-1} while the reorganization energy is 1011 cm^{-1}. Note that when using a smaller electronic coupling of 10 cm^{-1} instead in the present calculations, the effect of additional decoherence is found to be slightly stronger, agreeing with the findings by Landry and Subotnik.[34] The MFL method is found to work surprisingly well, deviating only very slightly from the SH and SHD results. The most obvious difference is obtained at the MF level, where the equilibrium populations do not converge to the thermodynamic limit of 0.5, in strong contract with all other approaches. In order to understand this difference, we also investigate the time evolution of the system kinetic energy, E_k, as predicted by the different approaches (see Fig. 3(b)). As expected, E_k in the SH and SHD approaches always fluctuates around $k_BT/2$ due to the inclusion of the system-bath interaction. For MFL, E_k decreases a little bit in the very beginning and goes back to $k_BT/2$ after 2 ps of dynamics simulation. This shows that electrons acquire energy from the nuclear vibrations to cross the barrier in the MF approaches, and inclusion of system-bath interactions enables the nuclei to maintain their kinetic energy.

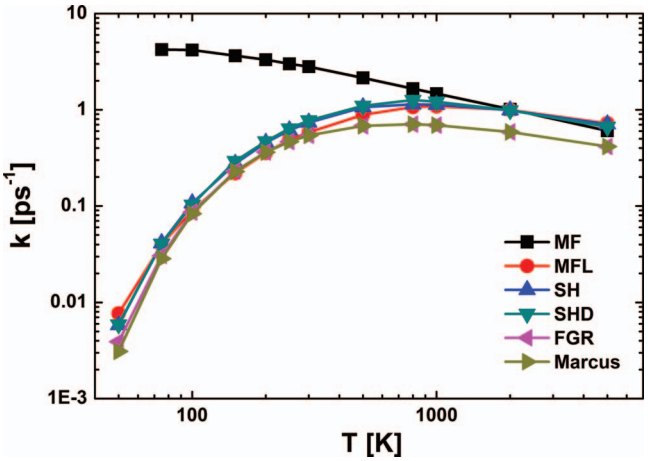

FIG. 4. Temperature dependence of the charge transfer rate by the MF approach with and without system-bath interaction, the SH approach with and without decoherence, together with the results from FGR and Marcus formula.

Without such system-bath interaction, the nuclei can lose about 30% of their kinetic energy (see Fig. 3(b)), so that the electron transfer freezes out as the nuclei energy decreases.

The temperature-dependence of charge transfer rate from the MF and SH approaches is shown in Fig. 4, together with the FGR and Marcus results. Marcus and FGR rates are very close to each other for the whole range of investigated temperatures, showing that quantum effects in the nuclear motion can be neglected (which is expected since the temperature dependence is dominated by the low frequency phonons here). Based on the parameters used in this study, the real decoherence time is calculated to be about 12 fs at 300 K,[40] which is much smaller than the hopping time, i.e., inverse of the charge transfer rate, about 2 ps, implying that MF is not principally applicable here. However, as found for the time evolution of charge population, SH, SHD, and MFL provide almost identical temperature dependent mobilities, in line with FGR and Marcus results. Considering the simplicity of MFL with respect to SH and SHD, MFL really does a great job in computing charge transfer rates for dimers. In contract, the result from MF is quite misleading: the rate decreases monotonously with temperature. Note that the SH calculations in the absence of system-bath interaction gives similar temperature dependent rates. This sheds light into the importance of including the system-bath interaction to get the correct trend for charge transfer rate in the MF approximation.

C. Charge transport mobility in molecular stacks

Again, we first examine the role of the friction factor γ on charge transport mobility at different temperatures. We take the MF theory starting from the charged geometry as an example, see Fig. 5(a). It is found that the mobility is generally γ-independent when $\gamma < 1$ ps^{-1}, and decreases for larger γ. This behavior is very similar to conclusions from a previous study.[22] In the following, we use $\gamma = 1$ ps^{-1} for MF and SH calculations with system-bath interaction. Besides, we find that the temperature dependence of mobility is quite similar for different γ values (see Fig. 5(b)). We have also carried out

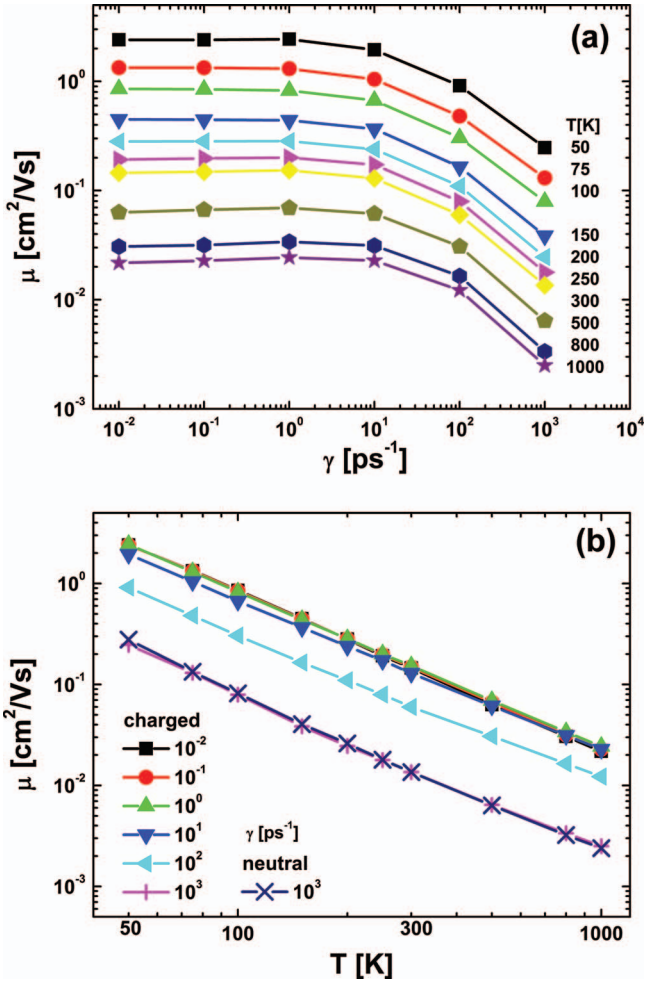

FIG. 5. (a) Friction and (b) temperature dependence of the charge transport mobility by the MF theory with system-bath interaction. The charged geometry was taken as the initial configuration for (a) and the indicated data points in (b). A test calculation was made in (b) using neutral initial geometry.

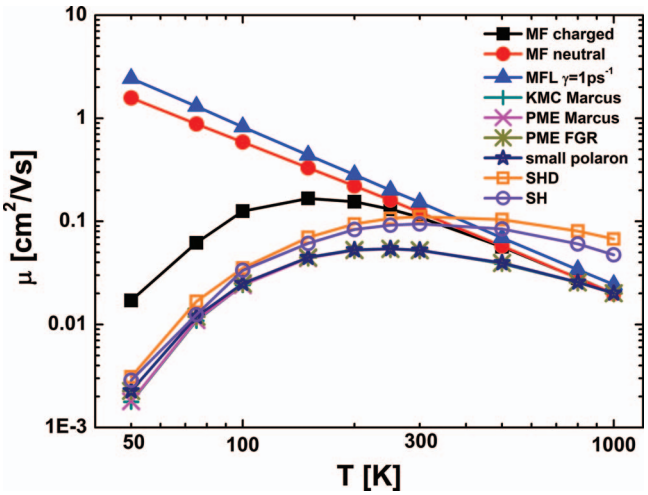

FIG. 6. Temperature dependence of mobility calculated with the MF theory starting from charged and neutral geometries without system-bath interaction, MF theory with system-bath interaction, the KMC and PME approaches based on Marcus charge transfer rate, the PME approach based on FGR, the small polaron model, and FSH calculations with and without decoherence. Only local electron-phonon couplings are considered.

a test study with the neutral geometry as initial condition and $\gamma = 10^3$ ps^{-1}, and found similar results, showing that the inclusion of system-bath interaction can wipe out the influence of different initial conditions. Here below, we discuss only the results obtained when using the charged geometry as initial nuclear coordinates while accounting for the system-bath interactions.

In Fig. 6, we compare the calculated temperature dependence of mobility with only local electron-phonon couplings from various approaches. As expected, the PME and KMC approaches using Marcus charge transfer rates give identical results. If FGR rates are used instead, the mobility values are just slightly larger at low temperature, similar to the findings for the charge transfer rate. The values obtained from small polaron theory are similar to the results of the PME simulations based on FGR charge transfer rates, due to the fact that both approaches use the same perturbation scheme in the small electronic coupling limit. SH and SHD are very close and agree very well with the PME/KMC calculations except at high temperatures. The MF mobility using charged geometry gives similar thermally activated temperature dependence but with larger values especially at low temperatures. In contract, the data obtained from the MF approach with neutral geometry at time zero follow a bandlike power law with temperature. This result agrees with previous studies with pure nonlocal electron-phonon couplings.[18] With system-bath interactions, the temperature dependence is just up-shifted, showing also a bandlike behavior.

In order to understand the different behaviors of MF approaches, we took several snapshots in the dynamics and obtained the transient mobility (according to the time-dependent slope of the MSD) as a function of temperature, see Fig. 7. For the MF approach including system-bath interaction, the mobility at short time scales is thermally activated and then changes to bandlike as time evolves. For MF approaches without system-bath interaction, the temperature dependence stays bandlike and thermally activated with neutral and charged initial geometries, respectively. Comparing MF approach with charged geometry with and without system-bath interaction, we conclude that the system-bath interactions play a role only at times longer than 10 ps. Note that the charge transport mobility is defined at the equilibrium diffusion at long time scales. As a result, their temperature dependence of mobility is significantly different (see Fig. 6).

We have also checked the time evolution of the charge population at different molecule sites. From Figs. 8(a) and 8(b), a difference is noticeable only at the first molecular site, namely, the molecule bearing the charge initially. As in the case of the charge transfer rate, this molecule gives away kinetic energy to the excess electron. In the absence of system-bath interaction, a thermal equilibrium is maintained between the electron and the nuclei of the first molecule. As a result, a large fraction of charge gets self-trapped on the first molecule. Thereby, the amount of charge that can escape from the first molecule needs to cross a barrier, thus implying thermally activated transport. From Fig. 8(b), the behavior of the escaped charges is similar for all MF approaches, and thus the obtained charge mobility is also thermally activated. With

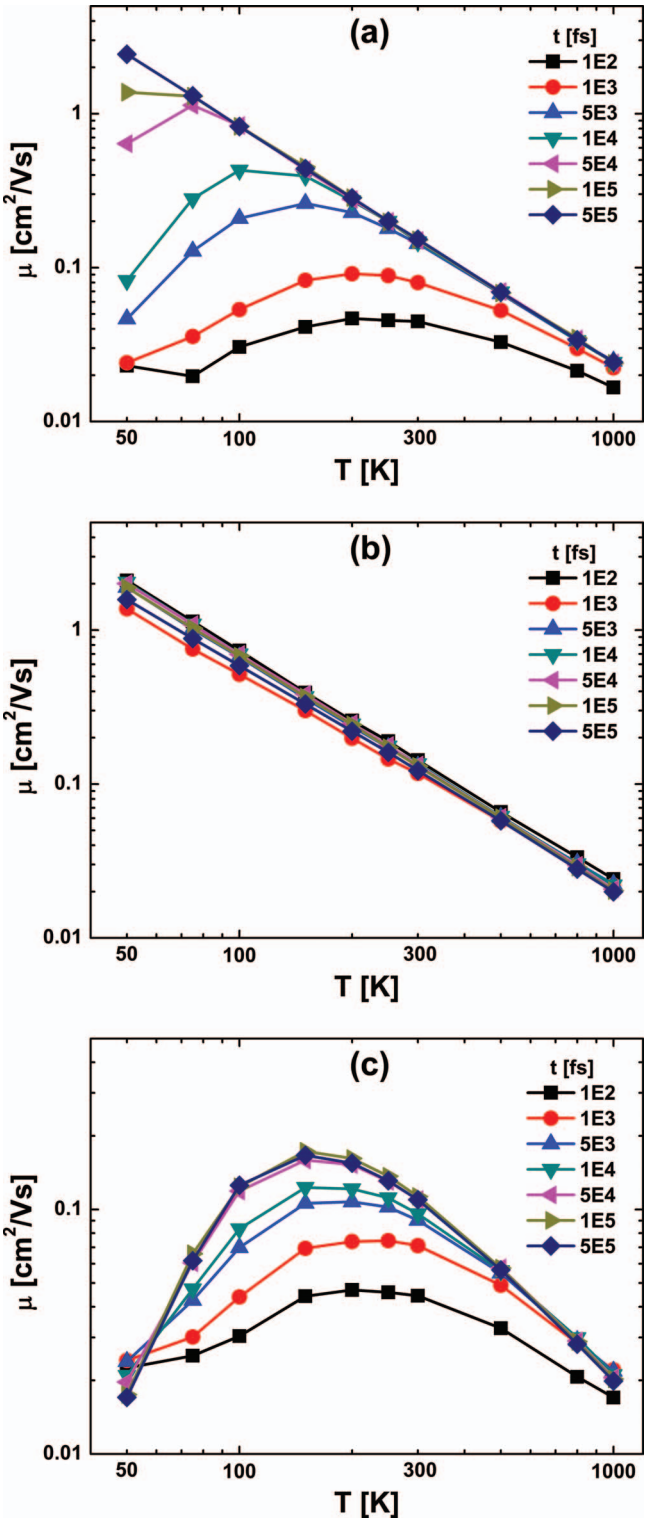

FIG. 7. Temperature dependence of charge transport mobility by (a) MF with system-bath interaction, and the MF theory starting from (b) neutral and (c) charged geometries without system-bath interaction. Only local electron-phonon couplings are considered. The mobilities estimated at different time scales are shown.

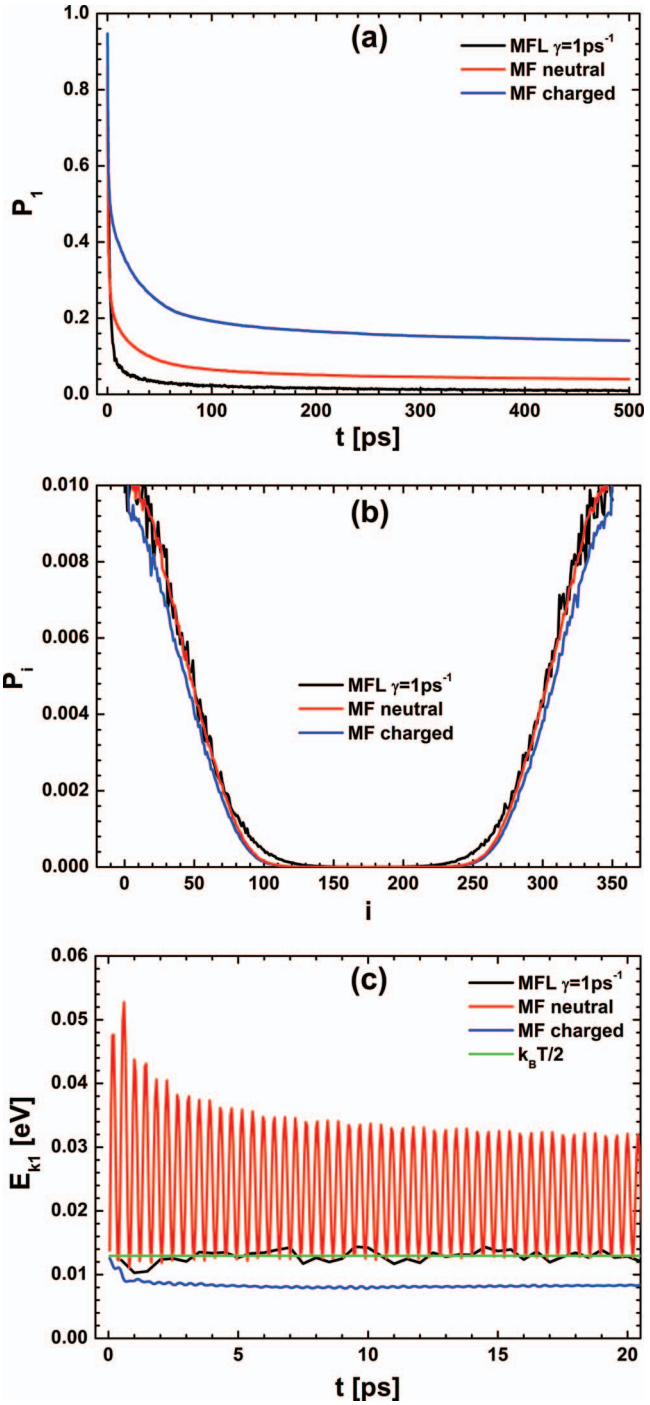

FIG. 8. (a) Time evolution of the charge population on the first molecule, (b) the charge distribution on other molecules at time 500 ps, and (c) time evolution of the kinetic energy of the first molecule by MF approach with system-bath interaction and MF approach starting from neutral and charged geometries in the absence of bath.

system-bath interaction, the charge is quite uniformly distributed over a lot of molecules, and thus the site energy for each molecule is very similar, resulting in a bandlike transport. For MF approach with neutral initial geometry, the kinetic energy fluctuates strongly with time, see Fig. 8(c). This is because the potential energy of a neutral molecule is much higher than that of a charged molecule and potential energy can be exchanged with kinetic energy for harmonic oscillators. This additional energy is enough to detrap the charge on the first molecule, and thus its transport behavior is similar to that with system-bath interactions.

Since the adopted parameters in this study can fully satisfy the condition to treat charge transport as a hopping

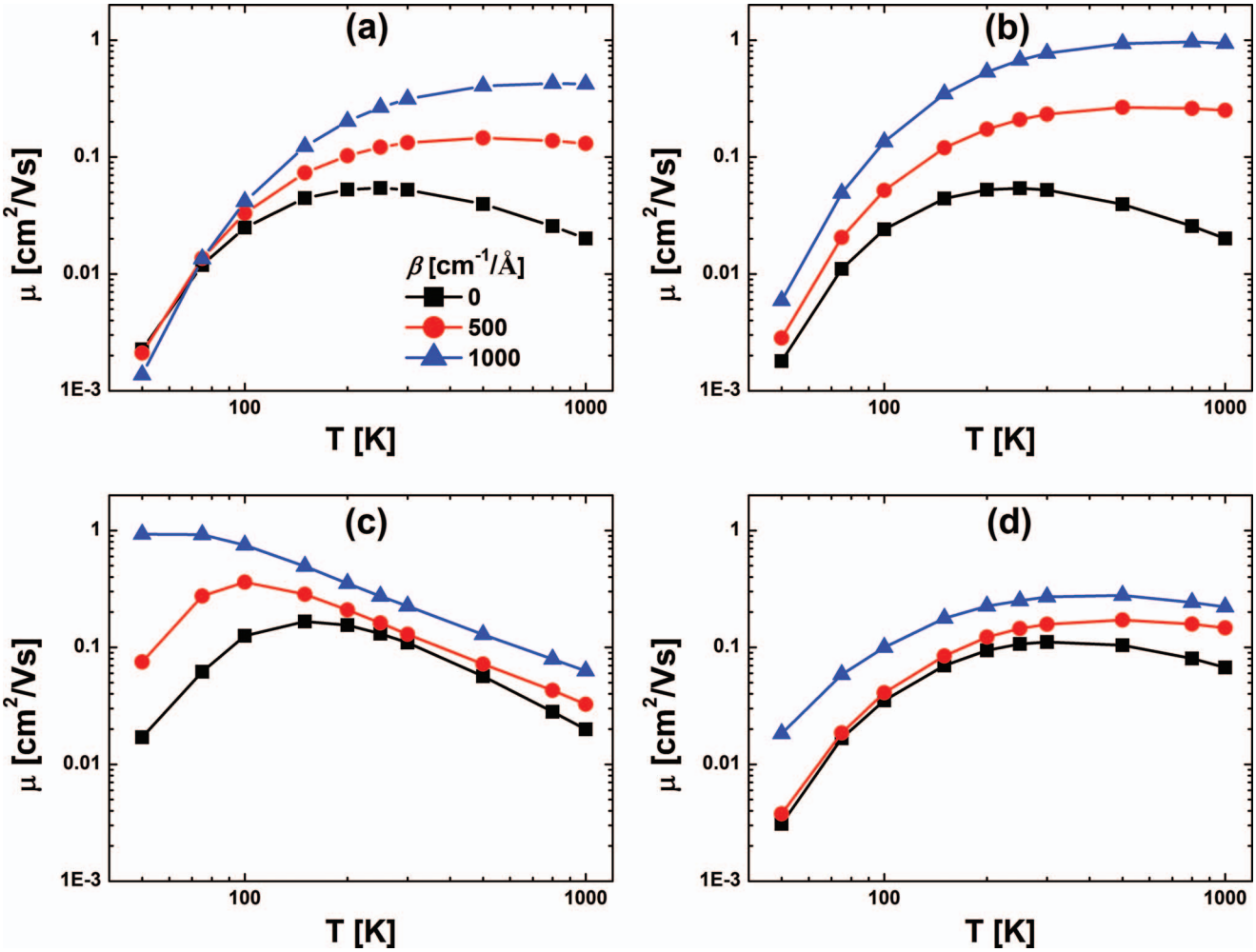

FIG. 9. Temperature dependence of charge transport mobility by (a) the small polaron model, (b) the PME with Marcus charge transfer rate, (c) the MF approach starting from charged geometries without system-bath interaction, and (d) FSH approach with decoherence. β varies as indicated.

process with Marcus charge transfer rate, the temperature dependence of mobility should be thermally activated as shown in Fig. 6. In this respect, the MF approach with neutral initial geometry in the absence of system-bath interaction should be used with caution, at least in case of materials with small charge carrier mobilities. Besides, the combination of the MF theory and system-bath interaction is not satisfying for charge transport due to its wrong long time behavior, although it works very well for charge transfer rates, where the short time behavior is important. At this stage, starting with the initial configuration of the charged molecule seems to be the only choice that can provide reasonable results within the scope of the MF level.

Finally, we study the role of additional nonlocal electron-phonon interaction on charge transport mobility within the small polaron model, the PME with Marcus charge transfer rate, the MF approach assuming an initially charged geometry, and the FSH technique (see Fig. 9). It is found that the small polaron mobility generally increases with the nonlocal electron-phonon coupling strength especially at high temperatures. Based on Eq. (18), the role of the nonlocal electron-phonon coupling is twofold: the total electron-phonon strength is increased due to the additional nonlocal electron-phonon couplings;[6] the nonlocal electron-phonon interactions add a thermally active term to the mobility.[3,7] Here, it seems that the latter effect exceeds the former. In the PME calculations, when the time cost for an intermolecular charge transfer is much slower than the vibrational period associated with the nonlocal electron-phonon coupling, the mean squared transfer integral should be used instead of the original transfer integral. Due to the Gaussian distribution of the transfer integral, $\langle V^2\rangle = \langle V\rangle^2 + \sigma_V^2$, where $\sigma_V = \sqrt{2\beta^2 k_B T/K}$ is the standard deviation of the transfer integral.[14] Thus, the mobility generally increases with the nonlocal electron-phonon coupling strength, as seen in Fig. 9(b). This behavior is similar to the small polaron theory but a larger enhancement is obtained. The mobility from the MF approach also increases monotonously with the nonlocal electron-phonon coupling strength (see Fig. 9(c)). However, the enhancement of the mobility is much stronger at low temperatures, suggesting that large nonlocal electron-phonon couplings are very helpful to detrap the localized charges. In the absence of local electron-phonon coupling,[18] it has been shown previously that the mobility should decrease with temperature since the translational symmetry of the electronic Hamiltonian is destroyed at higher temperatures. Here, we find that such

bandlike transport is also present even with strong local electron-phonon couplings when the nonlocal electron-phonon coupling is dominant. To get a clear picture of the role of the nonlocal electron-phonon coupling, we move to the SH approach (see Fig. 9(d)). There, when β is small, the low temperature dependence of mobility remains unchanged, and the mobility enhancement increases with temperature, similar to the small polaron result. As β is increased to 1000 $cm^{-1}/Å$, the curve is shifted upward, conserving the thermally activated temperature dependence. Overall, when both the local and nonlocal electron-phonon couplings are very large as studied here, the trend predicted by the polaron model should be generally correct and transport should be thermally activated. Thus, the prediction by the MF approach starting from charged geometry is problematic, and SH with nonadiabatic transitions must be used instead when studying charge transport in strongly disordered systems with mixed quantum-classical dynamics.

At last, we note that thermally activated transport in experiment can be widely found in materials based on thiophene, e.g., sexithiophenes,[47] which have large reorganization energy due to the flexibility of the inter-ring torsions. However, since large-size ultrapure molecular crystals are often hard to obtain, disorder may also play an important role in the measured temperature dependent mobilities.

IV. CONCLUSIONS

In this work, we have carefully investigated the performance of mean field theory against various other approaches in studying charge transfer rates between molecular dimers and charge transport mobility in molecular stacks. In the case of charge transfer, these include the quantum-mechanical Fermi Golden Rule, the semi-classical Marcus formula, the surface hopping approach with/without decoherence, as well as the mean field theory with/without system-bath interaction. For charge transport, we have considered the Pauli master equation and the kinetic Monte-Carlo simulation based on Fermi Golden Rule and Marcus charge transfer rates, the small polaron theory, the surface hopping with/without decoherence, as well as the mean field simulations with/without system-bath interaction for different initial conditions. We found that the mean field theory with system-bath interaction works very well for charge transfer rate, but fails completely for the temperature dependence of charge transport mobility in large systems. This is mainly because, while the mean field method is optimal at the short time scale relevant for the charge transfer rate, it is, however, no longer applicable at the longer times relevant to equilibrium charge transport mobility. Besides, it has been found that the real decoherence time is about two orders of magnitude smaller than the hopping time between neighboring molecules in the hopping regime of charge transport, hence the failure of the MF theory should be strongly related to the fact that it implies an infinitely long decoherence time. In contrast, surface hopping approaches, which naturally embody decoherence effects, generally work very well not only for the calculation of charge transfer rates but also for the simulation of charge transport dynamics.

ACKNOWLEDGMENTS

We thank Dr. Brain R. Landry and Professor Joseph E. Subotnik for helpful suggestions concerning the surface hopping simulations for charge transfer rate, and Professor Oleg V. Prezhdo for the discussion on decoherence time calculations. The work was supported by the Interuniversity Attraction Pole program of the Belgian Federal Science Policy Office (PAI 6/27), FNRS-FRFC, and the EC 7th Framework Program under Grant Agreement No. 212311 of the ONE-P project. D.B. is a FNRS Research Director.

APPENDIX: RK4 ALGORITHM TO SOLVE STOCHASTIC LANGEVIN EQUATIONS

We intend to solve the stochastic Langevin equation for a degree of freedom, x,

$$m\ddot{x} = -V' - \gamma m\dot{x} + \xi, \tag{A1}$$

where m is the effective mass, V' is the derivative of the potential energy with respect to the coordinate x, γ is the friction coefficient, ξ is a Markovian Gaussian random force with standard deviation $\sqrt{2\gamma m k_B T/\Delta t}$, k_B is the Boltzmann constant, T is the temperature, and Δt is the time interval of the dynamics. One first needs to use a standard RK4 algorithm[38] to calculate the coordinate and the velocity of a corresponding deterministic problem, x_{det} and v_{det},

$$m\dot{v}_{\text{det}} = -V' - \gamma m v, \tag{A2}$$

$$v_{\text{det}} = \dot{x}. \tag{A3}$$

Then the solution to the stochastic equation (Eq. (A1)) can be obtained by[39]

$$x = x_{\text{det}} + Z_2 - \gamma Z_3 + (-V''/m + \gamma^2)Z_4, \tag{A4}$$

$$v = v_{\text{det}} + Z_1 - \gamma Z_2 + (-V''/m + \gamma^2)Z_3 + (2\gamma V''/m - \gamma^3)Z_4. \tag{A5}$$

Here, V'' is the second derivative of the potential energy respect to the coordinate, $Z_1 = R_1$, $Z_2 = \Delta t \cdot (R_1/2 + R_2/2\sqrt{3})$, $Z_3 = \Delta t^2 \cdot (R_1/6 + \sqrt{3}/12 \cdot R_2 + R_3/12\sqrt{5})$, and $Z_4 = \Delta t^3 \cdot (R_1/24 + \sqrt{3}/40 \cdot R_2 + R_3/24\sqrt{5} + R_4/120\sqrt{7})$, where R_1, R_2, R_3, and R_4 are Gaussian random numbers with standard deviation $\sqrt{2\gamma k_B T \Delta t/m}$.

[1] T. Holstein, Ann. Phys. (N.Y.) **8**, 343 (1959).
[2] H. Sumi, J. Chem. Phys. **70**, 3775 (1979).
[3] R. W. Munn and R. Silbey, J. Chem. Phys. **83**, 1854 (1985).
[4] V. M. Kenkre, J. D. Andersen, D. H. Dunlap, and C. B. Duke, Phys. Rev. Lett. **62**, 1165 (1989).
[5] S. Fratini and S. Ciuchi, Phys. Rev. Lett. **91**, 256403 (2003).
[6] K. Hannewald and P. A. Bobbert, Appl. Phys. Lett. **85**, 1535 (2004).
[7] L. J. Wang, Q. Peng, Q. K. Li, and Z. Shuai, J. Chem. Phys. **127**, 044506 (2007).
[8] L. J. Wang, Q. K. Li, and Z. Shuai, J. Chem. Phys. **128**, 194706 (2008).
[9] Y.-C. Cheng and R. J. Silbey, J. Chem. Phys. **128**, 114713 (2008).
[10] F. Ortmann, F. Bechstedt, and K. Hannewald, Phys. Rev. B **79**, 235206 (2009).
[11] A. Troisi, Phys. Rev. B **82**, 245202 (2010).

[12]H. Bässler, Phys. Status Solidi B **175**, 15 (1993).
[13]G. J. Nan, X. D. Yang, L. J. Wang, Z. Shuai, and Y. Zhao, Phys. Rev. B **79**, 115203 (2009).
[14]L. J. Wang, Q. K. Li, Z. Shuai, L. P. Chen, and Q. Shi, Phys. Chem. Chem. Phys. **12**, 3309 (2010).
[15]D. Wang, L. P. Chen, R. H. Zheng, L. J. Wang, and Q. Shi, J. Chem. Phys. **132**, 081101 (2010).
[16]Y. C. Cheng, R. J. Silbey, D. A. da Silva Filho, J. P. Calbert, J. Cornil, and J.-L. Brédas, J. Chem. Phys. **118**, 3764 (2003).
[17]A. Troisi and G. Orlandi, J. Phys. Chem. A **110**, 4065 (2006).
[18]A. Troisi and G. Orlandi, Phys. Rev. Lett. **96**, 086601 (2006).
[19]M. Hultell and S. Stafström, Chem. Phys. Lett. **428**, 446 (2006).
[20]A. Troisi, Adv. Mater. **19**, 2000 (2007).
[21]A. Troisi, D. L. Cheung, and D. Andrienko, Phys. Rev. Lett. **102**, 116602 (2009).
[22]A. Troisi and D. L. Cheung, J. Chem. Phys. **131**, 014703 (2009).
[23]L. J. Wang, D. Beljonne, L. P. Chen, and Q. Shi, J. Chem. Phys. **134**, 244116 (2011).
[24]J.-L. Brédas, D. Beljonne, V. Coropceanu, and J. Cornil, Chem. Rev. **104**, 4971 (2004).
[25]V. Coropceanu, J. Cornil, D. A. da Silva Filho, Y. Olivier, R. Silbey, and J.-L. Brédas, Chem. Rev. **107**, 926 (2007).
[26]L. J. Wang, G. J. Nan, X. D. Yang, Q. Peng, Q. K. Li, and Z. Shuai, Chem. Soc. Rev. **39**, 423 (2010).
[27]Z. Shuai, L. J. Wang, and Q. K. Li, Adv. Mater. **23**, 1145 (2011).
[28]A. Troisi, Chem. Soc. Rev. **40**, 2347 (2011).
[29]P. Ehrenfest, Z. Phys. **45**, 455 (1927).
[30]J. C. Tully, in *Classical and Quantum Dynamics in Condensed Phase Simulations*, edited by B. Berne, G. Ciccotti, and D. F. Coker (World Scientific, Singapore, 1998).
[31]F. A. Bornemann, P. Nettesheim, and C. Schütte, J. Chem. Phys. **105**, 1074 (1996).
[32]O. V. Prezhdo and V. V. Kisil, Phys. Rev. A **56**, 162 (1997).
[33]J. C. Tully, J. Chem. Phys. **93**, 1061 (1990).
[34]B. R. Landry and J. E. Subotnik, J. Chem. Phys. **135**, 191101 (2011).
[35]S. H. Lin, C. H. Chang, K. K. Liang, R. Chang, Y. J. Shiu, J. M. Zhang, T. S. Yang, M. Hayashi, and F. C. Hsu, Adv. Chem. Phys. **121**, 1 (2002).
[36]R. A. Marcus, Rev. Mod. Phys. **65**, 599 (1993).
[37]L. J. Wang and D. Beljonne, J. Phys. Chem. Lett. **4**, 1888 (2013).
[38]W. H. Press, B. P. Flannery, S. A. Teukolsky, and W. T. Vetterling, *Numerical Recipes*, 2nd ed. (Cambridge University Press, Cambridge, 1992).
[39]E. Hershkovitz, J. Chem. Phys. **108**, 9253 (1998).
[40]A. B. Madrid, K. Hyeon-Deuk, and O. V. Prezhdo, ACS Nano **3**, 2487 (2009).
[41]H. J. Kreuzer, *Nonequilibrium Thermodynamics and Its Statistical Foundations* (Oxford University Press, New York, 1981).
[42]A. Einstein, Ann. Phys. **322**, 549 (1905).
[43]M. von Smoluchowski, Ann. Phys. **326**, 756 (1906).
[44]V. Chernyak and S. Mukamel, J. Chem. Phys. **112**, 3572 (2000).
[45]E. R. Bittner and P. J. Rossky, J. Chem. Phys. **103**, 8130 (1995).
[46]A. Nitzan, *Chemical Dynamics in Condensed Phase* (Oxford University Press, Oxford, 2006).
[47]L. Torsi, A. Dodabalapur, L. J. Rothberg, A. W. P. Fung, and H. E., Katz, Science **272**, 1462 (1996).